# Condensing water vapor to droplets generates hydrogen peroxide

Jae Kyoo Lee[a,1], Hyun Soo Han[b,c,1], Settasit Chaikasetsin[b], Daniel P. Marron[a], Robert M. Waymouth[a], Fritz B. Prinz[b,c,2], and Richard N. Zare[a,2]

[a]Department of Chemistry, Stanford University, Stanford, CA 94305; [b]Department of Mechanical Engineering, Stanford University, Stanford, CA 94305; and [c]Department of Materials Science and Engineering, Stanford University, Stanford, CA 94305

Contributed by Richard N. Zare, October 12, 2020 (sent for review September 25, 2020; reviewed by Raoul Kopelman and Veronica Vaida)

**It was previously shown [J. K. Lee *et al.*, *Proc. Natl. Acad. Sci. U.S.A.*, 116, 19294–19298 (2019)] that hydrogen peroxide ($H_2O_2$) is spontaneously produced in micrometer-sized water droplets (microdroplets), which are generated by atomizing bulk water using nebulization without the application of an external electric field. Here we report that $H_2O_2$ is spontaneously produced in water microdroplets formed by dropwise condensation of water vapor on low-temperature substrates. Because peroxide formation is induced by a strong electric field formed at the water–air interface of microdroplets, no catalysts or external electrical bias, as well as precursor chemicals, are necessary. Time-course observations of the $H_2O_2$ production in condensate microdroplets showed that $H_2O_2$ was generated from microdroplets with sizes typically less than ∼10 μm. The spontaneous production of $H_2O_2$ was commonly observed on various different substrates, including silicon, plastic, glass, and metal. Studies with substrates with different surface conditions showed that the nucleation and the growth processes of condensate water microdroplets govern $H_2O_2$ generation. We also found that the $H_2O_2$ production yield strongly depends on environmental conditions, including relative humidity and substrate temperature. These results show that the production of $H_2O_2$ occurs in water microdroplets formed by not only atomizing bulk water but also condensing water vapor, suggesting that spontaneous water oxidation to form $H_2O_2$ from water microdroplets is a general phenomenon. These findings provide innovative opportunities for green chemistry at heterogeneous interfaces, self-cleaning of surfaces, and safe and effective disinfection. They also may have important implications for prebiotic chemistry.**

microdroplet | water–air interface | hydrogen peroxide | vapor condensation | green Chemistry

Water molecules in liquid water are considered stable and inert. We and other investigators have reported that water molecules become electrochemically active and catalytic for various reactions when bulk water is formed into micrometer-sized droplets (microdroplets). Reaction rates for various chemical reactions are accelerated in microdroplets by factors of $10^2$ or more compared to bulk solution (1). The microdroplet environment provides conditions for a lowered entropic barrier, which allows thermodynamically unfavorable reactions to proceed in microdroplets at room temperature (2, 3). We also have shown that water microdroplets induce spontaneous charge exchanges between solutes and water molecules to induce the spontaneous reduction of organic molecules and metal ions as well as the formation of nanostructures without any added reducing agent or template (4, 5). Moreover, we have reported that water molecules undergo spontaneous oxidation to form reactive oxygen species, including hydroxyl radicals (OH) and hydrogen peroxide ($H_2O_2$) (6–8). Recent investigations attributed the origin of these unique physicochemical properties observed in microdroplets to the enrichment of reactants at the interface (9–11), restricted molecular rotations (12), partial solvation at the water surface (1, 13), and a strong interfacial electric field at the surface of the water microdroplet (14).

Microdroplets can be formed either by atomizing bulk water (top down) with various methods such as high-pressure gas nebulization (15), ultrasonic nebulization (16), vibrating micromesh nebulization (17), and piezoelectric nebulization (18), or by condensing vapor-phase molecules (bottom up) (19). A question may be asked whether those unique properties of microdroplets arise only in microdroplets formed by atomization of bulk water. In addition, it may be wondered whether the spontaneous oxidation of water to form $H_2O_2$ in microdroplets (6) was caused by the atomizing process involving friction or vibration. These questions motivated us to investigate whether $H_2O_2$ becomes spontaneously generated in water microdroplets formed by the condensation of water vapor in air on cold surfaces, and how universal might this process be. We have paid special attention to the influence of different surface properties, including hydrophilicity and surface roughness, as well as environmental factors, including relative humidity and surface temperature.

## Results

To test whether $H_2O_2$ can be generated in water microdroplets formed by condensation of water vapor in air on cold surfaces, we fabricated an environment control chamber that enables the control of relative humidity and temperature (Fig. 1). The relative humidity in the chamber was maintained by a feedback control loop consisting of a humidifier and a dehumidifier. The substrate temperature was manipulated with a Peltier cooler and an electric resistive heater, which were controlled by a feedback

### Significance

**Water molecules in bulk liquid are stable and inert under ambient conditions. In sharp contrast, we show that the condensation of water vapor in air to form microdroplets on cold surfaces causes the formation of hydrogen peroxide ($H_2O_2$) which we suggest is promoted by the large, intrinsic electric field at the air–water interface. This finding provides an alternative pathway for the production of atmospheric $H_2O_2$, for example, in raindrops as well as fogs and mists. This easy means of naturally producing $H_2O_2$ suggests many interesting possibilities, from the use of condensed steam for disinfection to how water microdroplets might have promoted formation of the building blocks of life in the prebiotic era.**

Author contributions: J.K.L., H.S.H., D.P.M., R.M.W., F.B.P., and R.N.Z. designed research; J.K.L., H.S.H., and S.C. performed research; J.K.L., H.S.H., and R.N.Z. analyzed data; and J.K.L., H.S.H., D.P.M., and R.N.Z. wrote the paper.

Reviewers: R.K., University of Michigan; and V.V., University of Colorado Boulder.

The authors declare no competing interest.



[1]J.K.L. and H.S.H. contributed equally to this work.

[2]To whom correspondence may be addressed. Email: fprinz@stanford.edu or zare@stanford.edu.

This article contains supporting information online at https://www.pnas.org/lookup/suppl/doi:10.1073/pnas.2020158117/-/DCSupplemental.

First published November 23, 2020.

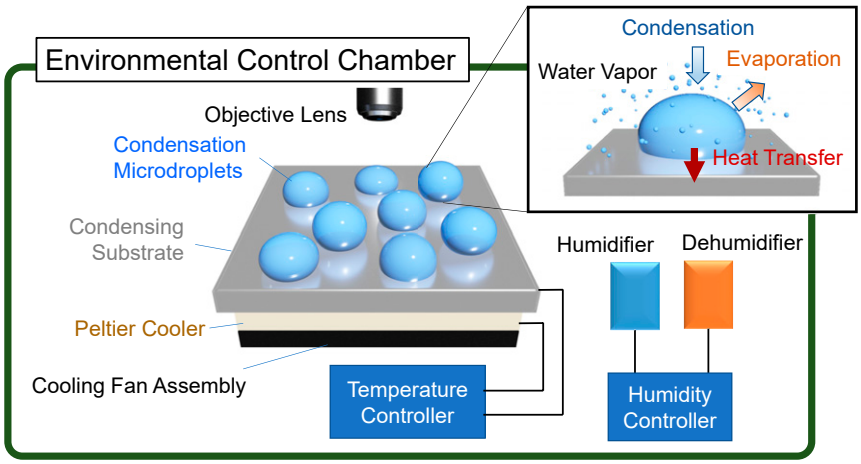


**Fig. 1.** Schematic of the experiment setup. An environmental control chamber was equipped with an automatic humidity control loop. The temperature of the substrate on which water vapor was condensed to form water microdroplets was controlled using a Peltier cooler and a resistive electric heater that were controlled by a feedback temperature controller. (*Inset*) Processes involved in the condensation of a microdroplet.

control loop. The chamber was also equipped with an optical microscope that enabled real-time imaging of microdroplet condensation. Because of the ease in collecting and assessing the size distribution of condensed microdroplets on solid surfaces compared to suspended microdroplets formed by the condensation of vapor nuclei, we studied microdroplet condensates formed on a cold surface rather than suspended microdroplets. We have chosen silicon (Si) as a model substrate because undoped single-crystalline Si offers low electric conductivity and, consequently, minimum interference to the formation of $H_2O_2$ (20). The Si wafer also has a reasonably high thermal conductivity that promotes the condensation of water vapor (21).

Fig. 2*A* shows a bright-field image of water microdroplet condensates formed on a precleaned Si wafer after 1-min cooling at 3.5 °C. The relative humidity in the environment control chamber was maintained at 55%. The average diameter of a water microdroplet was ∼4.6 ± 3.2 μm. To confirm that $H_2O_2$ is generated in condensed water microdroplets, we reacted collected water microdroplets on Si wafer surfaces with 4-carboxyphenylboronic acid. Fig. 2*B* presents the reaction scheme between 4-carboxyphenylboronic acid **1** and $H_2O_2$ to yield 4-hydroxybenzoic acid **2** and boric acid **3**. It also presents a mass spectrum showing reaction products between collected microdroplets and 4-carboxyphenylboronic acid. We observed the cleavage of reactant 4-carboxyphenylboronic acid (deprotonated, *m*/*z* 165.04) by $H_2O_2$ contained in microdroplets to produce 4-hydroxybenzoic acid **2** (deprotonated, *m*/*z* 137.02) and boric acid **3** (deprotonated, *m*/*z* 61.01). These results confirm the production of $H_2O_2$ in condensed water microdroplets.

To quantify the concentration of $H_2O_2$ generated in water microdroplets, we carried out a titration with potassium titanium oxalate (PTO, $K_2TiO(C_2O_4)_2 \cdot H_2O$). Fig. 2*C* shows the absorption spectra of 0.1 M PTO solution containing different concentrations of $H_2O_2$ as well as the collected water microdroplets. The calibration plot of the absorbance at 400 nm, acquired from Fig. 2*C*, shows the concentration of $H_2O_2$ generated in condensed water microdroplets to be ∼68 μM, which is ∼2.3 ppm (parts per million). The quantification was also performed using peroxide test strips (Movie S1). The agreement between the two different assays was confirmed in a previous study (6).

We recorded time-lapse imaging of microdroplet formation on a Si surface and compared the distribution of the microdroplet size with the $H_2O_2$ production yield to establish the relation between the two. Fig. 3 *A*–*C* shows the bright-field images and the size distribution of condensed water microdroplets at 0.5, 2, and 5 min after initiation of Si surface cooling at 3.5 °C. The relative humidity was maintained at 55%. Fig. 3*D* presents the $H_2O_2$ production yield as a function of time. At 0.5 min, the average microdroplet diameter was 4.0 ± 2.7 μm, and the $H_2O_2$ production yield was less than 1.0 ppm. Under continuous cooling, the microdroplet diameter increased to an average value of 7.7 ± 5.7 μm after 2 min. The $H_2O_2$ production yield reached a maximum value of ∼3.9 ppm at 2 min. After 5 min, microdroplets continued to grow with an average diameter of 12.5 μm. At this time point, droplets with diameters of ∼100 μm or larger were formed. Approximately 85% of the surface area was occupied by those large droplets or liquid films. Consequently, most of the liquid volume of collected microdroplets was dominated by these large droplets and liquid films. The concentration of the produced $H_2O_2$ at 5 min was reduced below the detection limit. A previous study using the $H_2O_2$-sensitive fluorescence dye, peroxyfluor-1, showed that $H_2O_2$ was mostly produced in water microdroplets less than 10 μm in diameter (6). This observation provides an explanation for why $H_2O_2$ production yield decreased when droplets continued to grow to form larger droplets or films, in which $H_2O_2$ is not effectively produced. The $H_2O_2$ produced at early time points when microdroplets are less than 10 μm becomes diluted, resulting in a decrease in the overall concentration. It may be desired to image microdroplets using $H_2O_2$-sensitive fluorescent dye, peroxyfluor-1, to establish a direct relationship between the microdroplet size and the $H_2O_2$ production yield. However, owing to the limitation of introducing dyes into microdroplets during condensation and the difficulty in normalizing the fluorescence intensity in growing droplets, this investigation could not be performed successfully.

To examine whether $H_2O_2$ can be formed on other surface types, we explored the production of $H_2O_2$ from water microdroplets condensed on plastic (Teflon), a glass slide, and polished copper. The surface temperature and the relative humidity were fixed at 3.5 °C and 55%. *SI Appendix*, Fig. S1*A* shows plots of $H_2O_2$ production yield on the different types of surfaces as a function of substrate cooling time. Although different surfaces exhibited different maximum $H_2O_2$ production yields, the qualitative temporal profiles remained almost the same, i.e., gradual rise and fall. The maximum $H_2O_2$ production yields are calculated from *SI Appendix*, Fig. S1*A*, showing that the Si wafer surface was the most efficient substrate for the production of $H_2O_2$ among the surfaces examined (*SI Appendix*, Fig. S1*B*). However, because these surfaces made of different materials have different physical properties such as surface roughness, hydrophobicity, and porosity, it could not be concluded whether the difference in the $H_2O_2$

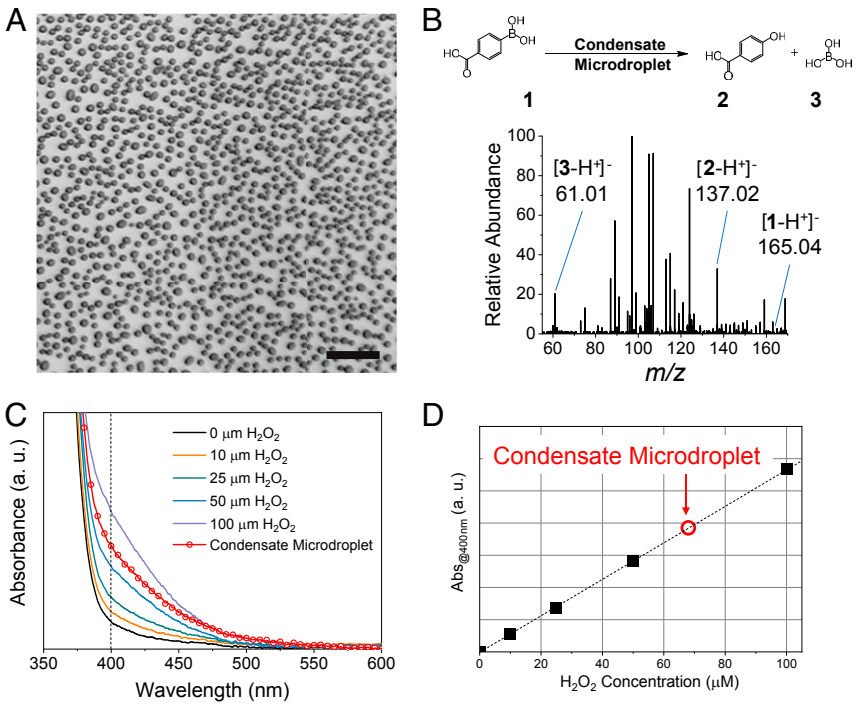


**Fig. 2.** Generation of hydrogen peroxide in water microdroplets formed by water-vapor condensation. (*A*) Bright-field image of microdroplets formed on the cooled Si wafer surface. (*B*) Mass spectrum showing reaction products from reacting carboxyphenylboronic acid **1** with $H_2O_2$ generated in condensed water microdroplets to form 4-hydroxybenzoic acid **2** and boric acid **3**. (*C*) The absorption spectrum of aqueous PTO solution with added $H_2O_2$ and a condensed microdroplet (red circle). (*D*) Calibration curve of the absorption at 400 nm acquired from spectra shown in *C*. The red circle represents the concentration of $H_2O_2$ generated from the condensed water microdroplet. (Scale bar, 50 μm.)

production yield arises from different chemical effects or different physical surface properties of the materials. Therefore, we measured the $H_2O_2$ production yield on the same Si substrate that had different surface properties prepared by different surface treatments.

To make a fair comparison of the effect of different types of surfaces on the $H_2O_2$ production yield, we prepared Si wafers that were prepared differently: 1) hydrophobic treated, 2) hydrophilic treated, and 3) plasma etched. We chose Si as a base substrate because of the availability of various surface modification methods and the chemical inertness of the Si surface.

For preparing a hydrophobic surface, we silanized Si wafer surfaces using 1,7-dichloro-octamethyltetrasiloxane ($Cl[Si(CH_3)_2O]_3Si(CH_3)_2Cl$) in heptane. The solvent and unbound residues were removed prior to condensation experiments. Fig. 4*A* shows a bright-field image of microdroplets condensed on a hydrophobic-treated Si surface taken at 2 min after the initiation of cooling. The number of microdroplets per unit area and the average microdroplet diameter were 18,709 per $mm^2$ and 4.3 ± 1.2 μm. These values were much lower than those values of 24,255/$mm^2$ and 7.7 ± 5.7 μm for microdroplets condensed on an untreated Si surface. This decrease in the formation of microdroplets on hydrophobic-treated surfaces might result in a decrease in the $H_2O_2$ production yield of 1.8 ppm at 2 min. The time-lapse images of microdroplets formed on the hydrophobic-treated Si wafer surface also showed that rates of both nucleation and droplet growth were slower compared to the untreated Si surface (*SI Appendix*, Fig. S2). This slow growth of microdroplets observed in images was consistent with the slow rise of $H_2O_2$ production yield shown in Fig. 4*D*.

We prepared a hydrophilic Si surface by treating Si surfaces with an oxygen plasma cleaner, which induces onto the Si surface hydrophilic groups such as oxygen atoms in Si–O–Si bonds (22). Because of the instability of the hydrophilic Si surface from the high-strength strain in Si–O–Si bonds, condensation experiments using oxygen plasma-treated Si surfaces were carried out no later than 30 min after the completion of the oxygen plasma treatment. Fig. 4*B* and *SI Appendix*, Fig. S3 show bright-field images of condensates formed on hydrophobic-treated Si surfaces. Notably, the Si surface was dominantly covered by thin films with lateral sizes over hundreds of micrometers, which was caused by the high wettability of the hydrophilic Si surface. In these water condensate films, no $H_2O_2$ was produced (Fig. 4*E*). There were thin films with a few micrometers in thickness and tens of micrometers in lateral diameter. It is unclear whether $H_2O_2$ can be formed in these micrometer-sized thin condensed water films because most of the liquid collected for quantitative analyses was dominated by larger thin films. Again, direct imaging of the $H_2O_2$ production in these individual condensates by employing, for instance, $H_2O_2$-sensitive fluorescent dyes, is necessary to determine the production of $H_2O_2$ in these thin water films.

Nucleation and growth of dropwise water condensation are promoted on surfaces with a higher surface roughness. We increased the roughness of the Si surface by treating it with deep reactive-ion etching technique in an inductive coupled plasma etcher. The etched Si surface exhibited an increased surface root-mean-square (rms) surface roughness of 3.80 nm compared to 0.12 nm on the untreated Si surface (*SI Appendix*, Fig. S4). Time-lapse images of bright-field images of the water condensation on etched Si surfaces show the formation of small nuclei as early as 15 s after the initiation of cooling, followed by a rapid increase of water condensation (*SI Appendix*, Fig. S5). Due to the increased wettability of the etched Si surface, thin liquid films were observed rather than microdroplets at and after 2 min. The time course of $H_2O_2$ concentration on etched Si surfaces exhibits a similar trend (Fig. 4*F*). The $H_2O_2$ production yield reached a maximum value at 30 s and decreased gradually afterward. These studies of the effect of the surface properties on

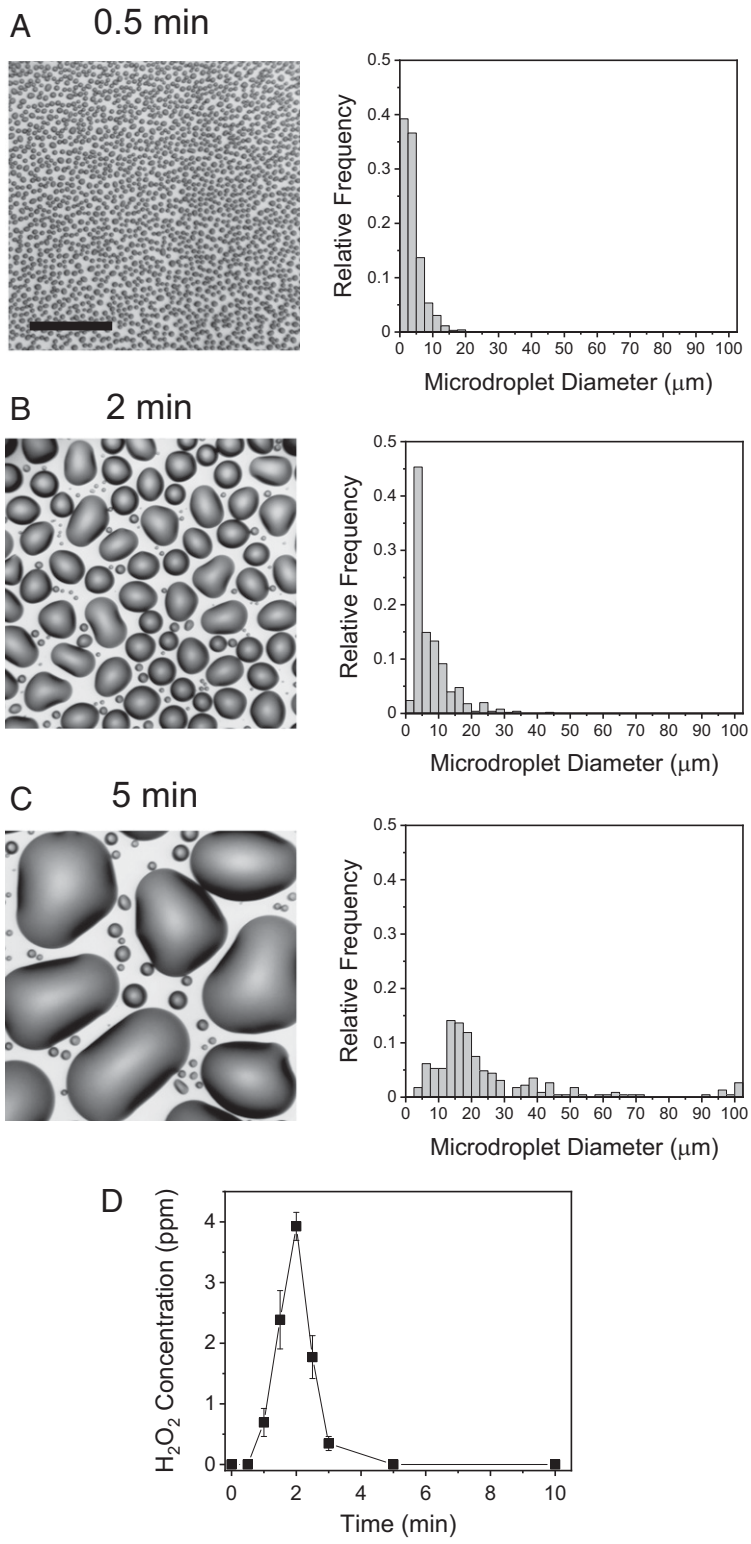


**Fig. 3.** Time course of $H_2O_2$ formation in condensed water microdroplets. Time-lapse bright-field images (*Left*) and size distribution (*Right*) of microdroplets formed on a Si wafer after (*A*) 0.5 min, (*B*) 2 min, and (*C*) 5 min of cooling with a Peltier cooler. (*D*) Time course of $H_2O_2$ concentration. Error bars represent 1 SD from three independent measurements. (Scale bar, 50 μm.)

the $H_2O_2$ production yield indicate that the nucleation and the growth of condensed microdroplets determine the $H_2O_2$ production yield. Particularly, the surface density of microdroplets less than ∼10 μm is important for achieving a high $H_2O_2$ production yield.

We also examined the dependence of $H_2O_2$ generation in condensed water microdroplets on environmental conditions, including relative humidity, ambient light level, and surface temperature. First, we measured the time course of $H_2O_2$ production yield under different relative humidity ranging from 40 to 70% in

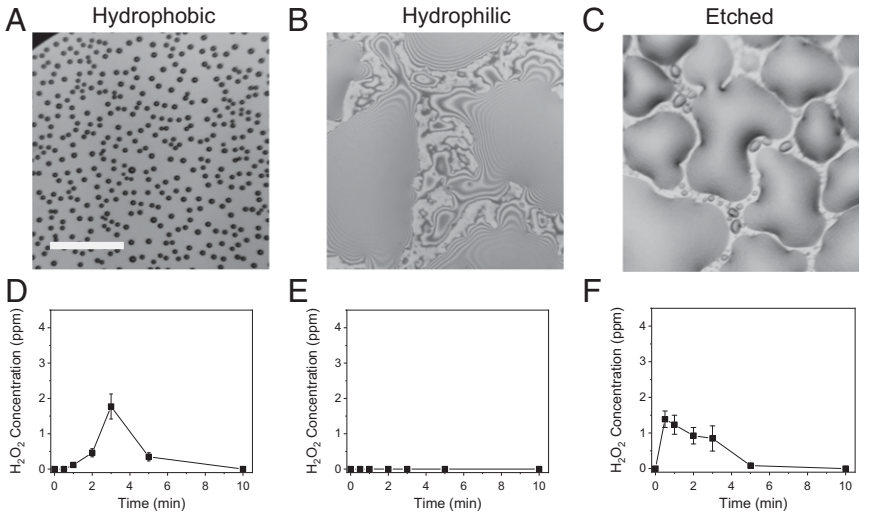


**Fig. 4.** Dependence of $H_2O_2$ production on surface treatment conditions. Si wafers were treated to be hydrophobic (*A* and *D*), hydrophilic (*B* and *E*), and etched for increased surface roughness (*C* and *F*). (*A*–*C*) Bright-field images taken at 2 min after the initiation of cooling. (*D*–*F*) Time courses of $H_2O_2$ concentration on each treated surface. Error bars represent 1 SD from three independent measurements. (Scale bar, 50 μm.)

the environment control chamber (Fig. 5*A*). The surface temperature of untreated Si water was kept at 3.5 °C. At 40% relative humidity, the growth of microdroplet formation became slower than at 55% and 70%. Consequently, the time point for the maximum $H_2O_2$ production yield was ∼3 min, which was slower compared to 2 min for the samples with 55 and 70% humidity. The time courses of $H_2O_2$ production yield under 55 and 70% humidity exhibit almost identical patterns, suggesting the $H_2O_2$ production was saturated beyond 55% relative humidity. These observations are also reflected in the plots of the maximum $H_2O_2$ production yield against relative humidity shown in Fig. 5*B*. The increase of relative humidity from 40 to 55% enhanced the $H_2O_2$ production yield from ∼0.5 to ∼4 ppm. The $H_2O_2$ production yield remains relatively constant above 55%.

We then explored the possible effect of visible-light irradiation on $H_2O_2$ production. *SI Appendix*, Fig. S6 shows there was almost no difference in the $H_2O_2$ production yield under different visible-light intensities from 0 to 4 mW/cm$^2$. This result indicates that the $H_2O_2$ generation from condensed water microdroplets was not induced or influenced by irradiation with visible light.

We also investigated the effect of the surface temperature at Si wafer surfaces on the $H_2O_2$ production yield (Fig. 5 *C* and *D*). The temperature of Si surfaces varied from −2.8 to 12.2 °C, while the relative humidity was fixed at 55%. Fig. 4*C* shows the time

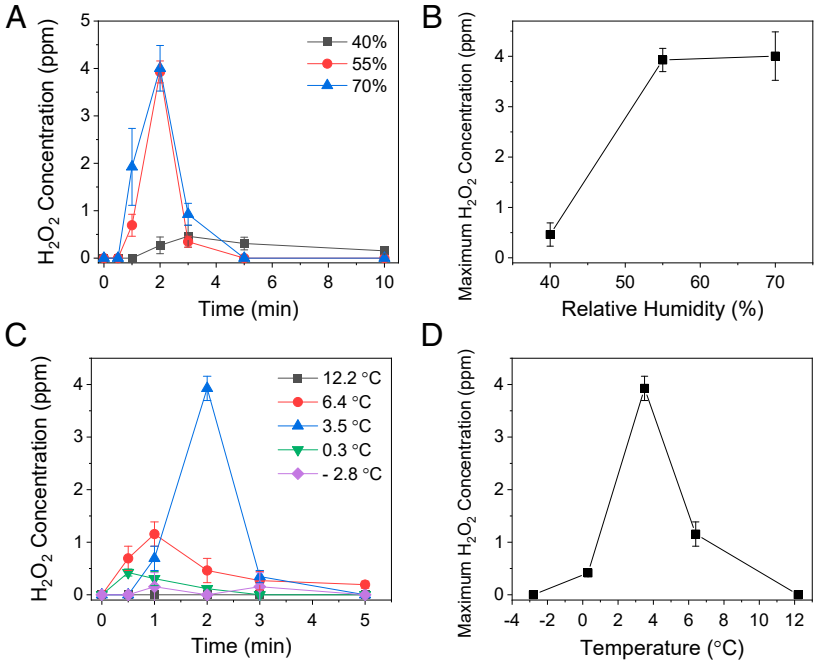


**Fig. 5.** Dependence of $H_2O_2$ generation from condensed water microdroplets on the relative humidity and the substrate temperature. (*A*) Time course of $H_2O_2$ concentrations on a bare Si wafer under different relative humidities. (*B*) Maximum $H_2O_2$ concentrations at different relative humidities. (*C*) Time course of $H_2O_2$ concentrations at different temperatures of a bare Si wafer (*D*) Maximum $H_2O_2$ concentrations at different surface temperatures of a bare Si wafer.

courses of $H_2O_2$ production yield under different temperatures. At −2.8 °C, condensed water was frozen to form thin ice layers at the surface, and no $H_2O_2$ production was detected. At 12.2 °C, almost no condensation occurred because of the lack of enough thermal gradient between water vapor, which was at room temperature, and the Si surface. The $H_2O_2$ production yield reached a maximum value of ∼3.9 ppm at 3.5 °C (Fig. 5*D*). These observations show that $H_2O_2$ production from condensed water microdroplets is sensitive to substrate surface temperature and humidity but not to ambient light levels.

## Discussion

We report the spontaneous production of $H_2O_2$ at several ppm levels in water microdroplets formed by the condensation of water vapor on low-temperature surfaces in air. The results in this work suggest that the spontaneous oxidation of water to form $H_2O_2$ in water microdroplets is a general phenomenon regardless of how microdroplets are created, either through condensation (bottom up) or atomization (top down). We found that the nucleation and growth processes are important for the $H_2O_2$ production yield because these processes determine the density and the size distribution of condensed water microdroplets. Surface temperature and relative humidity are also important factors influencing the production yield.

Although the maximum production yield and the time in which a maximum value appears to vary with the type of surfaces and with environmental factors such as temperature and relative humidity, the overall temporal profile of $H_2O_2$ production exhibits a bell-shaped behavior consisting of a simple rise and fall. This observation is consistent with our previous finding that $H_2O_2$ is dominantly produced in water microdroplets with diameters less than ∼10 μm (6). Fig. 6 *A*–*D* presents suggested processes explaining the typical rise and fall of $H_2O_2$ production in condensed water microdroplets. Before the initiation of surface cooling, water molecules in the vapor phase do not form any surface nuclei (Fig. 6*A*). No $H_2O_2$ is produced at this stage. As the surface temperature is lowered, small nuclei are formed on the cooled surface (Fig. 6*B*), and $H_2O_2$ starts being generated. Small nuclei grow to form microdroplets through different possible processes, including a simple growth, coalescence, and shedding of larger droplets onto smaller droplets (Fig. 6*C*). More $H_2O_2$ molecules are produced at this stage. It is unclear how these different routes for the growth of microdroplets influence the generation of $H_2O_2$ owing to the lack of a method for probing the production of $H_2O_2$ from individual microdroplets. As condensed water microdroplets continue to grow to form large droplets, the production of $H_2O_2$ decreases and then stops because the size of droplets becomes larger than the typical $H_2O_2$ production size limit, ∼10 μm (Fig. 6*D*). At this stage, $H_2O_2$ produced in previous stages is diluted; consequently, the overall concentration of $H_2O_2$ decreases. Eventually, condensed water forms thin liquid films on the surface, and the $H_2O_2$ concentration essentially drops below our detection limit.

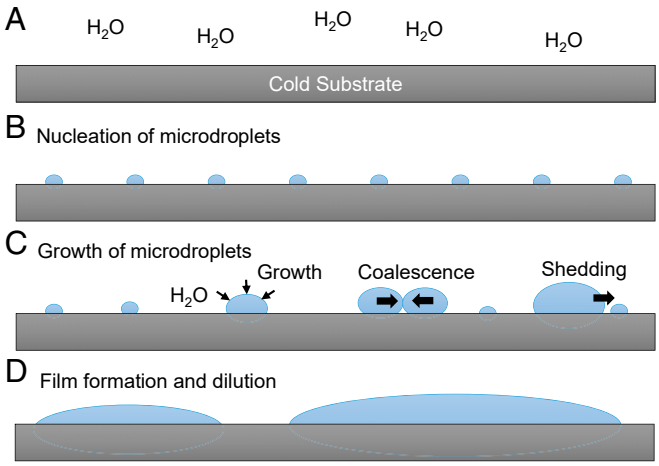


**Fig. 6.** Schematic of the time course of $H_2O_2$ formation on cold surfaces by condensation of water vapor: (*A*) capture of water vapor on cold substrate, (*B*) nucleation formation, (*C*) growth of microdroplets, and (*D*) formation of thin water film and the dilution of $H_2O_2$.

These observations provide a clue for enhancing the production yield of $H_2O_2$ beyond the ppm level. The increase of the density of micrometer-sized droplets with the delayed growth of these droplets through appropriate surface modification method (23) can lead to the improvement of the $H_2O_2$ production yield. This proposition was demonstrated by studies we made with modified Si surfaces, presented in Fig. 4. The etched Si surface exhibited a more rapid rise of $H_2O_2$ production yield to reach a maximum value as early as 30 s compared to 2 min in the untreated Si surface. A higher roughness of the etched Si surface (*SI Appendix*, Fig. S4), which promotes the nucleation (24), may be responsible for the rapid rise of the $H_2O_2$ concentration. However, the etched surface also increases surface wettability, which resulted in the formation of thin liquid films. Therefore, the overall $H_2O_2$ production yield decreased because of dilution of the previously produced $H_2O_2$ (*SI Appendix*, Fig. S5). In contrast, both nucleation and growth on the hydrophobic Si surface were inefficient compared to the bare Si surface, exhibiting the slower $H_2O_2$ formation with lower overall production yield. These observations suggested that to increase $H_2O_2$ yield, a better-designed structured surface is needed to promote the nucleation to form smaller droplets without having a liquid film being formed.

The mechanism for the formation of hydrogen peroxide in water microdroplets is presently not known, but some aspects seem well established. It has been shown that OH as well as other reactive oxygen species are present in freshly formed microdroplets (4, 6). It then seems reasonable to assume that $H_2O_2$ is formed from the recombination of OH radicals in water. The question is where does the OH come from? Many experiments have shown that water microdroplets surrounded by some hydrophobic medium, such as air or oil, are negatively charged (25, 26), although scrupulously purified water microdroplets are reported to be uncharged (27). The negatively charged water microdroplets have been attributed to the preferential adsorption of $OH^-$ at the interface (25, 28, 29), but this has been strongly disputed (30, 31). Another possibility for explaining negative charging is the preferential adsorption at the microdroplet periphery of some unknown anionic surfactant (32), such as the adsorption of bicarbonate anion ($HCO_3^-$) from the absorption by water of carbon dioxide ($CO_2$) by water microdroplets in contact with the air (27). Whatever the case, the presence of negatively charged ions at the interface causes the formation of an electric double layer, which in turn gives rise to a strong electric field. Recently, Xiong et al. (14) determined the electric field to be on the order of $10^7$ V/cm at the periphery of a water microdroplet in oil. This was accomplished by measuring the Stark shift of a probe molecule at the microdroplet interface compared to that at the center of the microdroplet. It might then be speculated that this strong electric field at the periphery of the water microdroplet assists the conversion of $OH^-$ to OH or promotes a reaction that forms OH. The answer to what is the origin of the OH in water is presently under investigation.

The findings in this work carry the following notable implications. Because the spontaneous water oxidation to generate hydrogen peroxide occurs in water microdroplets formed by the condensation of water vapor, this work provides evidence that the water oxidation in water microdroplets is not caused by any process involved in the atomization of bulk water, for instance, a high-pressure gas nebulization, the friction between water and

air, and the electrification of moving water flow over different materials. Because no complex equipment or series of chemical processes are necessary to produce $H_2O_2$ and only vapor water is needed as a raw material for the production of $H_2O_2$, this work may provide a simple and economical method for on-demand production of $H_2O_2$ and other reactive oxygen species, which can be used for green disinfection and sterilization of surfaces.

Moreover, this work may have important implications for atmospheric chemistry because it represents another possible source for making hydrogen peroxide that does not need radiation as a driving energy source. It is well known that rainwater contains $H_2O_2$ (33–35). We suggest that some of this might be produced simply by water vapor condensation. At first, it might be thought that the concentration of $H_2O_2$ is too small to be important, but if the $H_2O_2$ is removed by some chemical reaction, it will be regenerated on the surface of the microdroplet in air. We also note that upon visible and ultraviolet photolysis, $H_2O_2$ yields OH radicals. It is thought that hydrogen peroxide plays an important role in the troposphere, such as the photochemical oxidation of sulfur dioxide to sulfuric acid in the formation of acid rain (36).

We also wish to point out that the spontaneous formation of hydrogen peroxide in fogs, mists, and raindrops may be a missing part of the story of how the building blocks of life were formed on Earth. Clearly, this process can play an important role in redox chemistry without the need to have a biological catalyst present. It may also provide a new pathway for the origin of atmospheric oxygen on Earth. Conventionally, atmospheric oxygen is thought to originate in the photocatalytic splitting of vapor water (37). Because $H_2O_2$ self-decomposes into $H_2O$ and $O_2$, the results in this work suggest that water microdroplets, which are abundant in nature, might be an alternative source of atmospheric oxygen during the prebiotic era. This speculation is supported by our previous study reporting the generation of oxygen atoms in water microdroplets (5). In addition, the results of this study suggest that the biological ecosystem, particularly the microbiome, might be influenced by spontaneously generated reactive oxygen species in water microdroplets.

## Materials and Methods

**Chemicals.** High-performance liquid chromatography (HPLC)-grade water was purchased from Fisher Scientific Co. Potassium titanium oxalate [$K_2TiO(C_2O_4)_2 \cdot H_2O$] and 4-carboxyphenylboronic acid were purchased from Sigma-Aldrich.

**Microdroplet Generation and Characterization.** A custom-designed chamber was fabricated for maintaining environmental conditions, including temperature and relative humidity, for generating microdroplets formed by water vapor condensation. The surface temperature of wafers was maintained by polyimide resistive heater films and a thermoelectric Peltier cooling module (TEC1-12706), which were connected to a temperature controller (ITC-308, Inkbird Tech). The ∼10-g thermal compound paste was applied between the Peltier cooling module and a Si wafer to promote heat transfer. The relative humidity of the environment control chamber was manipulated using a household humidifier and a dehumidifier, which were connected to a programmable plug digital humidity controller (IHC-200, Inkbird Tech). The mist generated from the ultrasonic humidifier was placed away from the condensation module in order to avoid any direct deposit of droplets generated from the humidifier onto substrates. The microdroplet condensation chamber was equipped with an optical microscope (Nikon) for monitoring the condensation on substrates. Image analyses for the size distribution and the number of microdroplets were carried out using ImageJ (NIH). The visible-light irradiance of fluorescent room light and white-light light emitting diode light source was measured at 550 nm using a laser power meter (FieldMate 1098297, Coherent).

**Mass Spectrometric Analysis.** Thermo Scientific LTQ Orbitrap XL Hybrid Ion Trap-Orbitrap mass spectrometer was used for mass spectrometric analysis of the reaction products collected from the microdroplet condensate solution and 4-carboxyphenylboronic acid. The volume of 200 μl from the microdroplet condensate solution was mixed with 200 μl of 100 μM 4-carboxyphenylboronic acid to form a solution that was introduced into the mass spectrometer inlet without forming aerosol microdroplets in order to avoid possible reactions occurring in aerosol microdroplets. No voltage was applied to the solution. The heated capillary inlet to the mass spectrometer was maintained at ∼275 °C. The capillary and tube lens voltages were set as −44 and −60 V, respectively.

**Quantification of $H_2O_2$ Production.** The $H_2O_2$ concentration in microdroplets was determined by PTO and spectrophotometric analysis with a maximum response at 400 nm. A 0.1 M PTO ($K_2TiO(C_2O_4)_2 \cdot H_2O$; ≥99.0%, Sigma-Aldrich) solution was prepared. To develop the calibration curve, 200 μL of a $H_2O_2$ standard solution with a concentration between 0 and 100 μM was added into the 200-μL PTO solution. From this mixture, a 300-μL aliquot was removed, and the absorbance at 400 nm was measured using a Tecan Infinite M1000 Plate Reader (Tecan Benelux BVBA). An identical procedure was conducted on microdroplet samples where 200 μL of collected microdroplets was combined with PTO. The $H_2O_2$ concentration of microdroplet samples was determined from the calibration curve acquired from the standard $H_2O_2$ solution. The $H_2O_2$ concentration of microdroplets was also confirmed using peroxide test strips (Quantofix, Macherey-Nagel), which covered the range of 0.5–25 ppm $H_2O_2$.

**Si Surface Treatment.** Undoped Si wafers with 4-in. diameter and 500-μm thickness were used as a base substrate for studies about the dependence of surface conditions on the $H_2O_2$ production. Si waters were cleaned prior to each treatment. For preparing a hydrophobic Si surface, wafers were treated with Sigmacote (Sigma-Aldrich) following the manufacturer's protocol. Briefly, cleaned and dried wafers were covered with undiluted Sigmacote solution for 30 min at room temperature and air dried. Treated wafers were rinsed three times with HPLC-grade water and dried before condensation experiments. Hydrophilic Si wafers were prepared by treating precleaned wafers in an oxygen plasma cleaner at 30 W for 30 s. Hydrophilic wafers were used for condensation experiments within 30 min after the plasma treatment. Etched Si wafers were prepared by deep reactive-ion etching in an inductive coupled plasma (ICP) etcher from Plasma-Therm at the Stanford Nanofabrication Facilities. The samples are etched for 100 cycles using a standard recipe with a Si etch rate of 0.83 μm/cycle without any mask. Each cycle of the recipe includes three main steps: 1) deposition of polymer step (150 sccm of C4F8, 30 sccm of Ar, 25 mTorr, 2,000-W ICP power, 10-V bias voltage, 2.5 s); 2) polymer etch A step (150 sccm SF6, 30 sccm Ar, 40 mTorr, 2,000-W ICP power, 250-V bias voltage, 1.5 s); and 3) Si etch B step (300 sccm SF6, 30 sccm Ar, 75 mTorr, 3,000-W ICP power, 10-V bias voltage, 3.0 s). The pressure of the backside He was maintained at 4 Torr, while temperatures of the electrode, liner, lid, and spool were kept at 15, 70, 150, and 180 °C, respectively.

**Roughness Measurement.** The sample roughness measurement was carried out with an atomic force microscope tool from Park XE-70 system at the Stanford Nano Shared Facilities. Standard NSC15 cantilever probe with a typical resonance frequency of 325 kHz and a spring constant of 40 N/m were used in noncontact mode.

**Data Availability.** All study data are included in the article and *SI Appendix*.

**ACKNOWLEDGMENTS.** H.S.H. acknowledges support from the Volkswagen Group of America. This work was funded by the Air Force Office of Scientific Research through Basic Research Initiative Grant AFOSR FA9550-12-1-0400.

1. Z. Wei, Y. Li, R. G. Cooks, X. Yan, Accelerated reaction kinetics in microdroplets: Overview and recent developments. *Annu. Rev. Phys. Chem.* **71**, 31–51 (2020).
2. I. Nam, J. K. Lee, H. G. Nam, R. N. Zare, Abiotic production of sugar phosphates and uridine ribonucleoside in aqueous microdroplets. *Proc. Natl. Acad. Sci. U.S.A.* **114**, 12396–12400 (2017).
3. I. Nam, H. G. Nam, R. N. Zare, Abiotic synthesis of purine and pyrimidine ribonucleosides in aqueous microdroplets. *Proc. Natl. Acad. Sci. U.S.A.* **115**, 36–40 (2018).
4. J. K. Lee, D. Samanta, H. G. Nam, R. N. Zare, Micrometer-sized water droplets induce spontaneous reduction. *J. Am. Chem. Soc.* **141**, 10585–10589 (2019).
5. J. K. Lee, D. Samanta, H. G. Nam, R. N. Zare, Spontaneous formation of gold nanostructures in aqueous microdroplets. *Nat. Commun.* **9**, 1562 (2018).
6. J. K. Lee *et al*., Spontaneous generation of hydrogen peroxide from aqueous microdroplets. *Proc. Natl. Acad. Sci. U.S.A.* **116**, 19294–19298 (2019).
7. F. Jin, D. Gao, J. K. Lee, R. N. Zare, Aqueous microdroplets containing only ketones or aldehydes undergo Dakin and Baeyer–Villiger reactions. *Chem. Sci. (Camb.)* **10**, 10974–10978 (2019).
8. M. T. Dulay *et al*., Spraying small water droplets acts as a Bacteriocide. *Q. Rev. Biophys. Discovery* **1**, 1–8 (2020).

9. Z. Zhou, X. Yan, Y.-H. Lai, R. N. Zare, Fluorescence polarization anisotropy in microdroplets. *J. Phys. Chem. Lett.* **9**, 2928–2932 (2018).
10. A. Fallah-Araghi *et al*., Enhanced chemical synthesis at soft interfaces: A universal reaction-adsorption mechanism in microcompartments. *Phys. Rev. Lett.* **112**, 028301 (2014).
11. S. Lhee *et al*., Spatial localization of charged molecules by salt ions in oil-confined water microdroplets. *Sci. Adv.* **6**, eaba0181 (2020).
12. J. Kang, S. Lhee, J. K. Lee, R. N. Zare, H. G. Nam, Restricted intramolecular rotation of fluorescent molecular rotors at the periphery of aqueous microdroplets in oil. *Sci. Rep.*, **10**, 16859 (2020).
13. S. Mondal, S. Acharya, R. Biswas, B. Bagchi, R. N. Zare, Enhancement of reaction rate in small-sized droplets: A combined analytical and simulation study. *J. Chem. Phys.* **148**, 244704 (2018).
14. H. Xiong, J. K. Lee, R. N. Zare, W. Min, Strong electric field observed at the interface of aqueous microdroplets. *J. Phys. Chem. Lett.* **11**, 7423–7428 (2020).
15. R. Wang *et al*., The role of nebulizer gas flow in electrosonic spray ionization (ESSI). *J. Am. Soc. Mass Spectrom.* **22**, 1234–1241 (2011).
16. S. Kooij, A. Astefanei, G. L. Corthals, D. Bonn, Size distributions of droplets produced by ultrasonic nebulizers. *Sci. Rep.* **9**, 6128 (2019).
17. O. Z. Olszewski *et al*., A silicon-based MEMS vibrating mesh nebulizer for inhaled drug delivery. *Procedia Eng.* **168**, 1521–1524 (2016).
18. S. V. Minov, F. Cointault, J. Vangeyte, J. G. Pieters, D. Nuyttens, Droplet generation and characterization using a piezoelectric droplet generator and high speed imaging techniques. *Crop Prot.* **69**, 18–27 (2015).
19. M. Ahlers, A. Buck-Emden, H.-J. Bart, Is dropwise condensation feasible? A review on surface modifications for continuous dropwise condensation and a profitability analysis. *J. Adv. Res.* **16**, 1–13 (2018).
20. S. Suh, H. Choi, K. Eom, H.-J. Kim, Enhancing the electrochemical properties of a Si anode by introducing cobalt metal as a conductive buffer for lithium-ion batteries. *J. Alloys Compd.* **827**, 154102 (2020).
21. H. Shanks, P. Maycock, P. Sidles, G. Danielson, Thermal conductivity of silicon from 300 to 1400 K. *Phys. Rev.* **130**, 1743 (1963).
22. S. B. Habib, E. Gonzalez, R. F. Hicks, Atmospheric oxygen plasma activation of silicon (100) surfaces. *J. Vac. Sci. Technol.* **28**, 476–485 (2010).
23. J. Su, M. Charmchi, H. Sun, A study of drop-microstructured surface interactions during dropwise condensation with quartz crystal microbalance. *Sci. Rep.* **6**, 35132 (2016).
24. M. D. Mulroe, B. R. Srijanto, S. F. Ahmadi, C. P. Collier, J. B. Boreyko, Tuning superhydrophobic nanostructures to enhance jumping-droplet condensation. *ACS Nano* **11**, 8499–8510 (2017).
25. K. Roger, B. Cabane, Why are hydrophobic/water interfaces negatively charged? *Angew. Chem. Int. Ed. Engl.* **51**, 5625–5628 (2012).
26. J. K. Beattie, A. M. Djerdjev, G. G. Warr, The surface of neat water is basic. *Faraday Discuss.* **141**, 31–39, discussion 81–98 (2009).
27. A. P. Carpenter, E. Tran, R. M. Altman, G. L. Richmond, Formation and surface-stabilizing contributions to bare nanoemulsions created with negligible surface charge. *Proc. Natl. Acad. Sci. U.S.A.* **116**, 9214–9219 (2019).
28. J. K. Beattie, A. M. Djerdjev, The pristine oil/water interface: Surfactant-free hydroxide-charged emulsions. *Angew. Chem. Int. Ed. Engl.* **43**, 3568–3571 (2004).
29. C. Bai, J. Herzfeld, Surface propensities of the self-ions of water. *ACS Cent. Sci.* **2**, 225–231 (2016).
30. C. J. Burnham, M. K. Petersen, T. J. F. Day, S. S. Iyengar, G. A. Voth, The properties of ion-water clusters. II. Solvation structures of $Na^+$, $Cl^-$, and $H^+$ clusters as a function of temperature. *J. Chem. Phys.* **124**, 024327 (2006).
31. R. J. Saykally, Air/water interface: Two sides of the acid-base story. *Nat. Chem.* **5**, 82–84 (2013).
32. Y. Uematsu, D. J. Bonthuis, R. R. Netz, Impurity effects at hydrophobic surfaces. *Curr. Opin. Electrochem.* **13**, 166–173 (2019).
33. P. Tanner, A. Y. S. Wong, Spectrophotometric determination of hydrogen peroxide in rainwater. *Anal. Chim. Acta* **370**, 279–287 (1998).
34. Y. Deng, Y. Zuo, Factors affecting the levels of hydrogen peroxide in rainwater. *Atmos. Environ.* **33**, 1469–1478 (1999).
35. Y. F. Fang, Y.-P. Huang, G.-F. Luo, R.-P. Li, [Determination of hydrogen peroxide in rainwater by fluorometry]. *Guang Pu Xue Yu Guang Pu Fen Xi* **28**, 917–921 (2008).
36. S. A. Penkett, B. M. R. Jones, K. A. Brice, A. E. J. Eggleton, The importance of atmospheric ozone and hydrogen peroxides in cloud and rainwater. *Atmos. Environ.* **13**, 123–137 (1979).
37. J. F. Kasting, J. L. Siefert, Life and the evolution of Earth's atmosphere. *Science* **296**, 1066–1068 (2002).